Gas Separation

DOI: 10.1002/anie.201003723

CO_2-Stable and Cobalt-Free Dual-Phase Membrane for Oxygen Separation**

Huixia Luo, Konstantin Efimov, Heqing Jiang, Armin Feldhoff, Haihui Wang, and Jürgen Caro**

The increase in carbon dioxide emissions is considered to be the main contribution to global warming. Therefore, there is an urgent need to reduce the emissions of CO_2 into the atmosphere. Recently, CO_2 capture and storage technologies to reduce the CO_2 emissions from coal-fired power plants have gained the attention of decision makers in governments, industry, and academia. There are three major concepts for CO_2 sequestration: post-combustion capture, pre-combustion separation, and oxyfuel techniques.[1] MIECMs, which are ceramic membranes with mixed oxygen ionic and electronic oxygen conductivity, have gained increasing attention owing to their potential applications in oxygen supply[2] to power stations for CO_2 capture according to the oxyfuel concept.[3] This concept involves burning natural gas with nitrogen-free oxygen, thus allowing CO_2 to be sequestered after steam condensation. Dense MIECMs are promising candidates for this oxygen separation from air. However, when MIECMs are used for this purpose, some of the CO_2 is recycled and used as the sweep gas for the oxygen separation, simultaneously lowering the temperature in the burner. Furthermore, CO_2-stable MIECMs could be promising for dry reforming and the thermal decomposition of carbon dioxide in combination with the partial oxidation of methane to syngas.[4]

Many complex oxides have been investigated as membranes for oxygen separation and in membrane reactors. However, there are two main problems for the proper application of this kind of membrane. First, perovskite membranes with cobalt doping usually show high permeability but poor stability under harsh working conditions;[5] by avoiding cobalt, the stability of MIEC membrane materials can be enhanced.[6] Second, for numerous applications such as the oxyfuel process or hydrocarbon partial oxidations, where some CO_2 is formed as a byproduct of an undesired deeper oxidation, the oxygen transporting membranes must sustain their phase stability and oxygen transport properties. Usually, the perovskite-type membranes contain alkaline earth metal ions on the A site, such as barium and strontium, which tend to react with CO_2 and form carbonates.[7] However, when using perovskites as oxidation catalysts, the negative effect of CO_2 as product molecule can be reduced if the reaction is carried out in a microwave field.[8,9] Also in the case of CO_2 decomposition with a hydrocarbon as oxidant on the other side of the MIECM, the negative influence of CO_2 can be reduced. The aforementioned problems can be overcome by using a cobalt-free and alkaline-earth-metal-free dual-phase membrane, which is composed of two interpenetrating percolated networks of an oxygen conductor (solid oxide electrolyte) and an electron conductor (internally short-circuiting electrode). In an extension of this concept, the dual phases might also consist of MIECMs with deviating transfer rates for oxygen and electrons.[10]

The first dual-phase membranes were made of oxygen conductors and noble metals: $(Bi_2O_3)_{0.74}SrO_{0.26}$-Ag,[11] $Bi_{1.5}Y_{0.3}Sm_{0.2}O_3$-Ag,[12] $Bi_{1.5}Er_{0.5}O_3$-Ag,[13] $Bi_{1.6}Y_{0.4}O_3$-Ag,[14] and YSZ-Pd.[15] However, the application of these materials is limited owing to high materials costs, a mismatch of the coefficient of thermal expansion (CTE) between the ceramic and metallic phases, and poor oxygen permeabilities. In another concept, perovskite- or fluorite-type oxides are used instead of noble metals as electron conductors.[16–18] However, these dual-phase membranes have a perovskite phase as electron conductor in which the A site is often occupied by alkaline earth metals, which can be easily eroded by forming carbonates if CO_2 is present. Improved stability against carbonate formation can be expected if both phases are made from oxides, which contain only transition metals and/or lanthanides. Both groups of elements are very tolerant against carbonate formation as shown by thermodynamics as well as by gravimetric considerations.[19,20]

Herein, we have prepared a novel alkaline-earth-free CO_2-stable and cobalt-free composite dual-phase membrane containing 40 wt% $NiFe_2O_4$ with a spinel structure and 60 wt% $Ce_{0.9}Gd_{0.1}O_{2-\delta}$ with a fluorite structure (abbreviated as 40NFO–60CGO). In the mixture of the two phases, NFO is the electron conductor and CGO is the oxygen-ion conductor. Phase structure and stability and also oxygen permeability were investigated under different atmospheres at high temperatures. Special attention is paid to the CO_2 stability.

The dual phase membrane was synthesized using powder mixing and the one-pot method. X-ray diffraction (Figure 1)

[*] H. Luo, K. Efimov, Dr. H. Jiang, Dr. A. Feldhoff, Prof. Dr. J. Caro
Institute for Physical Chemistry and Electrochemistry
Leibniz University Hannover
Callinstrasse 3–3A, 30167 Hannover (Germany)
Fax: (+49) 511-762-19121
E-mail: juergen.caro@pci.uni-hannover.de
Prof. Dr. H. Wang
School of Chemistry & Chemical Engineering
South China University of Technology
No. 381 Wushan Road, Guangzhou 510640 (China)
Fax: (+86) 20-8711-0131
E-mail: hhwang@scut.edu.cn

[**] H.L. acknowledges the financial support by the China Scholarship Council (CSC) and K.E. and A.F. thank the State of Lower Saxony for the NTH bottom-up grant no. 21-71023-25-7/09. H.W. is grateful for financial support from the NSFC (no. 20706020 and U0834004) and the 973 Plan (no. 2009CB623406). The authors also acknowledge F. Steinbach and F. Liang for technical support.

Supporting information for this article is available on the WWW under http://dx.doi.org/10.1002/anie.201003723.

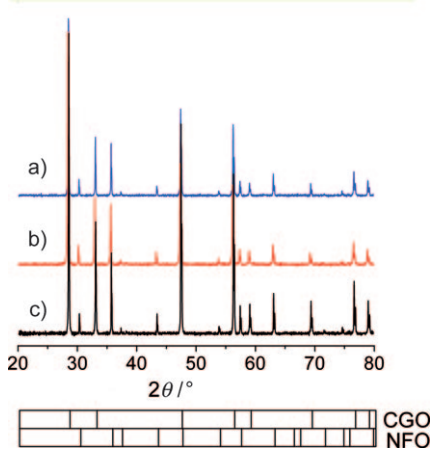

Figure 1. XRD pattern of 40NFO–60CGO membranes prepared by different methods and sintered at 1350 °C for 10 h in air. a) Mixing NFO and CGO powders by hand; b) direct one-pot method; c) spent one-pot membrane after the CO_2 stability test shown in Figure 6.

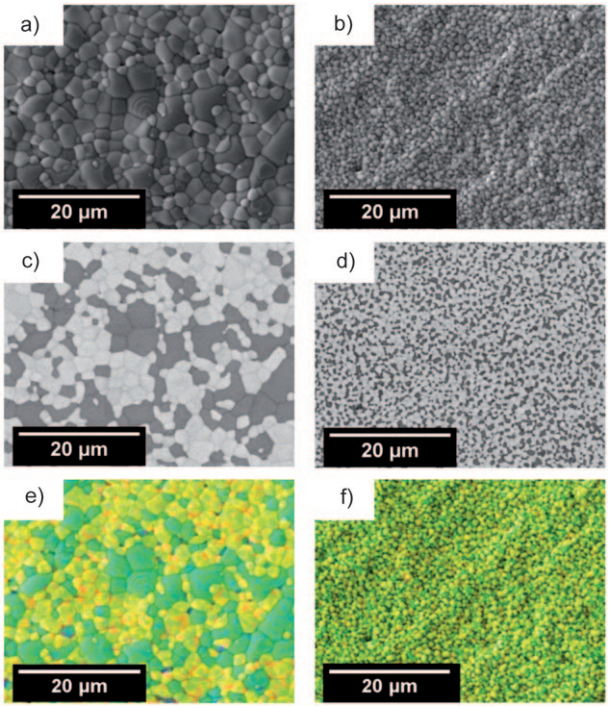

Figure 2. Grain structure of the surface (top view) of the 40NFO–60CGO composite membrane after sintering at 1350 °C for 10 h and prepared by different methods. Left line: powder mixing in a mortar by hand (a,c,e); right line: direct one-pot method (b,d,f). a,b) SEM, c,d) BSEM, e,f) EDXS.

clearly confirmed that both 40NFO–60CGO membranes consist of only the two phases NFO and CGO. The unit-cell parameter of the pure phases NFO (0.83455 nm) and CGO (0.54209 nm) are almost the same as in the 40NFO–60CGO dual-phase material (NFO: 0.83350 nm, CGO: 0.54186 nm). The phase composition was stable with time. As an example, Figure 1c shows the XRD of the spent 40NFO–60CGO membrane after the long-term oxygen separation with CO_2 as sweep gas (Figure 6).

Figure 2 shows the results of scanning electron microscopy (SEM), back-scattered SEM (BSEM), and energy-dispersive X-ray spectroscopy (EDXS) of both membranes. For the membrane prepared by powder mixing (Figure 2a,c,e), the grain size of CGO in these composite membranes is smaller (2–4 μm) than that of NFO (3–7 μm). BSEM in particular (Figure 2c) shows that there is clustering of grains of one and the same type; that is, NFO-NFO and CGO-CGO aggregation. In comparison to powder mixing, the membrane prepared by the direct one-pot method shows much smaller grains and a higher homogenization of the NFO and CGO phases (Figure 2b,d,f). The NFO and CGO grains could be distinguished by BSEM and EDXS. The dark grains in BSEM are NFO and the light grains are CGO, as the contribution of the back-scattered electrons to the SEM signal intensity is proportional to the atomic number. The same information is provided by EDXS. The green color (dark in the black-and-white version) is an overlap of the Fe and Ni signals, whereas the yellow color (light) stems from an average of the Ce and Gd signals.

In situ XRD provides an effective and direct way to characterize the high-temperature structure changes while increasing and decreasing temperatures under certain gas atmospheres. The in situ XRD patterns of the one-pot 40NFO–60CGO in air upon increasing and decreasing the temperature from 30 °C to 1000 °C and back to 30 °C (Supporting Information, Figure S1) indicate that the CGO and NFO phases remain unchanged in the 40NFO–60CGO dual-phase materials. During the oxygen supply for coal-based power stations, the membrane would be exposed to CO_2. Therefore, the high-temperature phase stability in a CO_2-containing atmosphere was studied by in situ XRD (Supporting Information, Figure S2). The in situ XRD patterns of 40NFO–60CGO dual-phase membranes between room temperature and 1000 °C in an atmosphere of 50 vol % CO_2 and 50 vol % N_2 (Supporting Information, Figure S2) shows that the composite membrane retains its dual phases over the entire temperature range. In an atmosphere of 50 vol % CO_2 and 50 vol % N_2, no carbonate formation could be detected. These results show that the composite membrane 40NFO–60CGO is stable in a CO_2 atmosphere. The time dependence of the oxygen flux with pure CO_2 as sweep gas also confirmed that the dual-phase membrane was CO_2-stable (Figure 6).

The scanning transmission electron microscope (STEM) high-angle annular dark-field (HAADF) micrograph in Figure 3a and also the EDXS elemental distributions in Figure 3c reveal a clear phase separation of CGO and NFO in the membrane. The grain size can be determined from these figures to be in the range of 500 nm to 1 μm, which is in accordance with the SEM findings. Similar to BSEM (Figure 2c,d), in the STEM-HAADF micrograph the dark grains are NFO and light grains are CGO (Figure 3a). The electron energy-loss (EEL) spectra (Figure 3b) were taken from circa 150 nm circular areas in the volume of CGO (top) and NFO grains (bottom). The fine-structure of the O_K ionization edge is characteristic to the respective oxide. No intermixing of cations between the two phases can be observed (that is, CGO

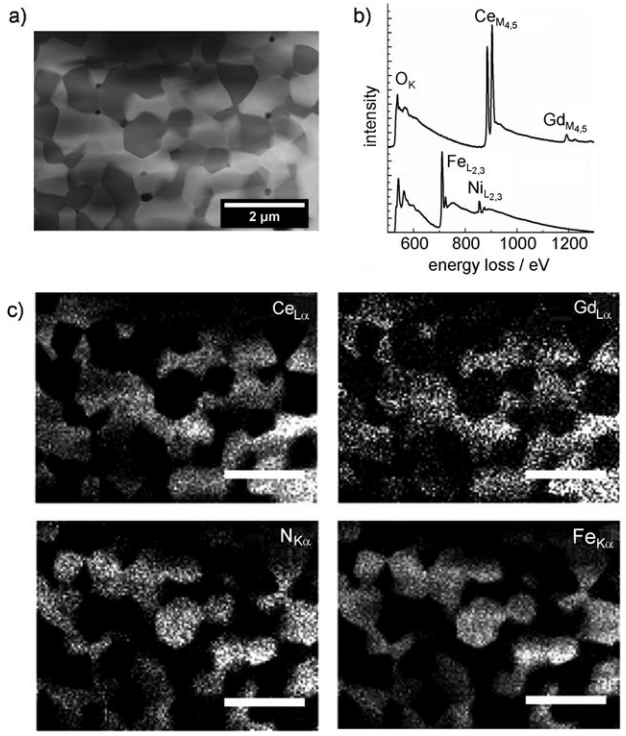

Figure 3. a) STEM-HAADF micrograph of a dual-phase membrane obtained by the direct one-pot method, showing CGO by bright contrast and NFO by dark contrast. Very dark contrast corresponds to holes in the as-prepared specimen. b) EEL spectra from the grain volume of CGO and NFO giving clear indication of phase separation. c) EDXS elemental distributions of Ce, Gd, Ni, and Fe. Scale bars: 2 μm.

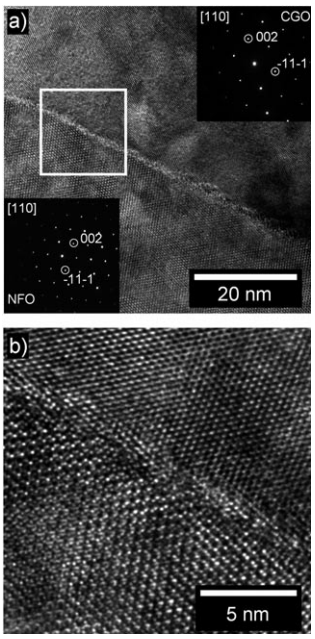

Figure 4. HRTEM of a CGO–NFO contact in a dual-phase membrane that was obtained from the direct one-pot method. a) Medium magnification with SAED pattern as insets (CGO at top, NFO at bottom); b) close-up of the marked area in (a).

contains neither Fe nor Ni, and NFO contains neither Ce nor Gd), which shows that a dual-phase membrane with well-separated grains was obtained by the direct one-pot method.

Figure S3a in the Supporting Information shows a CGO–CGO interface with the grain to the left being imaged along $[111]_{CGO}$ zone axis and the grain to the right exhibiting $(111)_{CGO}$ planes. Figure S3b in the Supporting Information shows an NFO–NFO interface with both grains exhibiting $(202)_{NFO}$ lattice planes. In both cases of interfaces between grains of the same kind, the grains are in intimate contact with no interphase between them, which is obvious from the HRTEM micrographs of Figure S3. This result was supported by EDXS and EELS, which could not identify any Fe or Ni at CGO–CGO interfaces and no Ce or Gd at NFO–NFO interfaces.

Figure 4 displays a contact between grains of different type (CGO and NFO). The grain at top is CGO imaged along the $[110]_{CGO}$ zone axis, and the grain at bottom is NFO imaged along $[110]_{NFO}$ zone axis (see the selected-area electron diffraction (SAED) pattern as insets in Figure 4a). Some Moiré fringes are noted in the right part of Figure 4a, which appear to be due to a slight inclination of the grain boundary with respect to the electron beam and give rise to a circa 1 nm-thick bright contrast feature along the whole grain boundary. Figure 4b shows a close-up of the marked area in Figure 4a and gives no indication of any interphases. Locally varying phase contrast in Figure 4a and b can be attributed to changes in the thickness of the as-prepared TEM specimen after ion sputtering. Thus, it is concluded that all interfaces in the dual-phase membrane, which was obtained from direct one-pot method, exhibit well-separated grains in intimate contact.

Figure 5 shows the oxygen permeation fluxes of our dual phase composite membranes prepared by the one-pot method, and by mixing the powders by hand in a mortar, using He and CO_2, respectively, as sweep gases. For the membrane prepared by one-pot synthesis, oxygen permeation fluxes of 0.31 and 0.27 $mL\,min^{-1}\,cm^{-2}$ are found at 1000 °C when pure He and CO_2 are used as sweep gases.

If the two powders NFO and CGO are mixed by hand in a mortar, only 50 % of the oxygen permeances of the one-pot membrane are obtained (Figure 5). This experimental finding clearly indicates that a homogeneous grain size distribution and a small grain size are a condition for high oxygen fluxes, as mentioned before by Yang[21] who reported that the uniformity of dual-phase membrane effects the oxygen permeability. However, when pure CO_2 was taken as the sweep gas, the oxygen permeation flux was only slightly decreased (Figure 5), which demonstrates the high CO_2 stability of the material. On the other hand, there is a slight but remarkable reduction of the oxygen flux when CO_2 instead of He is used as sweep gas. This experimental finding can be explained by the inhibiting effect of carbon dioxide on the oxygen surface exchange reaction; that is, the presence of CO_2 decreases the rate of the oxygen release from the solid. This assumption is in complete agreement with previous findings,[22] which state that the oxygen surface-exchange reaction is not the same under different gas atmospheres. From an Arrhenius plot of the oxygen permeation fluxes when He and CO_2 were applied as sweep gases, the apparent

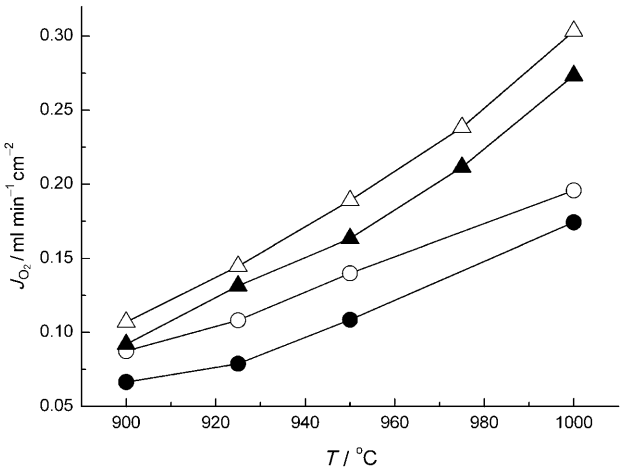

Figure 5. Oxygen flux J_{O_2} of 40NFO–60CGO dual-phase membranes prepared by different methods, and with a thickness of 0.5 mm, at different temperatures and with CO_2 and He as sweep gases. The air flow on the feed side was always $F_{air} = 150$ mL min^{-1}, the sweep flow was always 30 mL min^{-1}. He sweep with $F_{He} = 29$ mL min^{-1}, $F_{Ne} = 1$ mL min^{-1}: △ = one-pot membrane, ○ = powder mixing. CO_2 sweep with $F_{CO_2} = 29$ mL min^{-1}, $F_{Ne} = 1$ mL min^{-1}: ▲ = one-pot membrane, ● = powder-mixing method.

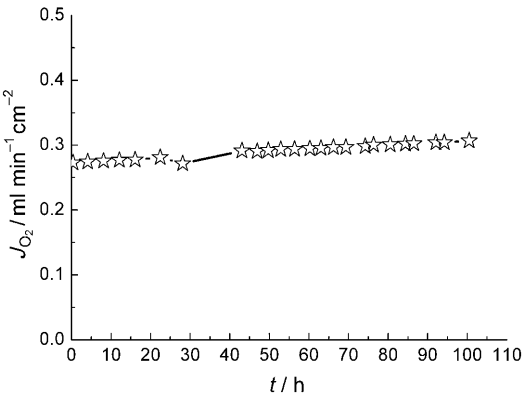

Figure 6. Oxygen permeation flux J_{O_2} through the 40NFO–60CGO composite membrane, prepared by the one-pot method, as a function of time at 1000 °C. Conditions: 29 mL min^{-1} CO_2 as sweep gas, 1 mL min^{-1} Ne as internal standard gas, 150 mL min^{-1} air as feed gas.

activation energies $E_a = (128 \pm 4)$ kJ mol^{-1} were found to be the same for the two membrane preparations within experimental error. Tong et al.[23] reported that a single activation energy is an important feature for a good stability of oxygen permeation through a oxygen membrane. In our case, a single activation energy was found in the range of 900–1000 °C.

The effect of the sweep rate on the oxygen permeation flux at temperature 1000 °C is shown in Supporting Information, Figure S4. Even when using CO_2 as the sweep gas, we observe the usual behavior, namely that oxygen permeances increase if the gradient of the oxygen partial pressure across the membrane is increased; this increase can be achieved by off-transporting the permeated oxygen as fast as possible, which can be realized with an increased sweep flow.

Figure 6 shows the long-term behavior of oxygen permeation flux through 40NFO–60CGO composite membrane at 1000 °C. During this oxygen permeation test, an oxygen permeation flux of about 0.30 mL min^{-1} cm^{-2} was obtained at 1000 °C, and no decrease of the oxygen permeation flux was found during the permeation test. After the oxygen permeation test, the sample was characterized by XRD (Figure 1 c). The dual-phase structure was retained, which indicates that 40NFO–60CGO exhibits excellent structure stability under a CO_2 atmosphere. The result is in agreement with the finding of in situ high-temperature XRD, indicating that the membrane is CO_2-stable. It is not like $Ba_{0.5}Sr_{0.5}Fe_{0.8}Zn_{0.2}O_{3-\delta}$ (BSFZ) or $Ba_{0.5}Sr_{0.5}Co_{0.8}Fe_{0.2}O_{3-\delta}$ (BSCF) perovskite materials, where carbonate was formed when CO_2 was the feed gas and the oxygen flux decreased rapidly.[7]

In conclusion, a novel CO_2-stable and cobalt-free dual-phase membrane of the composition 40 wt % $NiFe_2O_4$–60 wt % $Ce_{0.9}Gd_{0.1}O_{2-\delta}$ (40NFO–60CGO) was synthesized by a direct one-pot method, and for comparison by powder mixing in a mortar. In situ high-temperature X-ray diffraction demonstrated that the two phases NFO and CGO were stable upon repeated heating and cooling cycles between room temperature and 1000 °C in air and in an atmosphere with 50 vol % CO_2 and 50 vol % N_2. Energy-dispersive X-ray spectroscopy and back-scattered electron microscopy showed that the one-pot synthesis results in a dual-phase membrane with smaller NFO or CGO grains of uniform size distribution without homoaggregation of grains of the same phase, in comparison with a dual-phase membrane prepared by mixing the two powders. At 1000 °C, oxygen permeation fluxes of 0.31 and 0.27 mL min^{-1} cm^{-2} were obtained on the membrane prepared with the one-pot material for the sweep gases He and CO_2, respectively. This value is comparable with that of $La_2NiO_{4+\delta}$ and of $La_2Ni_{0.9}Fe_{0.1}O_{4+\delta}$, which are promising CO_2-stable membrane materials.[24] In a 100 h oxygen permeation using CO_2 as the sweep gas, no decline of the oxygen permeation flux was found, thus indicating that our dual phase membrane is CO_2-stable.

Received: June 18, 2010
Revised: August 30, 2010
Published online: December 22, 2010

Keywords: carbon dioxide · membranes · oxide membranes · oxygen separation

[1] R. Kneer, D. Toporov, M. Förster, D. Christ, C. Broeckmann, E. Pfaff, M. Zwick, S. Engels M. Modigell, *Energy Environ. Sci.* **2010**, *3*, 198–207.

[2] a) H. Q. Jiang, Z. W. Cao, S. Schirrmeister, T. Schiestel, J. Caro, *Angew. Chem.* **2010**, *122*, 5790–5794; *Angew. Chem. Int. Ed.* **2010**, *49*, 5656–5660; b) H. Q. Jiang, H. H. Wang, F. Y. Liang, S. Werth, T. Schiestel, J. Caro, *Angew. Chem.* **2009**, *121*, 3027–3030; *Angew. Chem. Int. Ed.* **2009**, *48*, 2983–2986; c) H. Q. Jiang, H. H. Wang, S. Werth, T. Schiestel, J. Caro, *Angew. Chem.* **2008**, *120*, 9481–9484; *Angew. Chem. Int. Ed.* **2008**, *47*, 9341–9344; d) H. H. Wang, Y. Cong, W. S. Yang, *Chem. Commun.* **2002**, 1468–1469; e) H. Q. Jiang, F. Y. Liang, O. Czuprat, K. Efimov, A. Feldhoff, S. Schirrmeister, T. Schiestel, H. H. Wang, J. Caro, *Chem. Eur. J.* **2010**, *16*, 7898–7903; f) H. Q. Jiang, L. Xing, O. Czuprat, H. H. Wang, S. Schirrmeister, T. Schiestel, J. Caro,

Chem. Commun. **2009**, 6738 – 6740; g) J. Pérez-Ramírez, B. Vigeland, *Angew. Chem.* **2005**, *117*, 1136 – 1139; *Angew. Chem. Int. Ed.* **2005**, *44*, 1112 – 1115.

[3] a) H. H. Wang, S. Werth, T. Schiestel, J. Caro, *Angew. Chem.* **2005**, *117*, 7066 – 7069; *Angew. Chem. Int. Ed.* **2005**, *44*, 6906 – 6909; b) G. A. Richards, K. H. Casleton, B. T. Chorpening, *Proc. IMechE Part A* **2005**, *219*, 121 – 126; c) S. Rezvani, Y. Huang, D. McIlveen-Wright, N. Hewitt, J. D. Mondol, *Fuel* **2009**, *88*, 2463 – 2472; d) B. J. P. Buhre, L. K. Elliott, C. D. Sheng, R. P. Gupta, T. F. Wall, *Prog. Energy Combust. Sci.* **2005**, *31*, 283 – 307.

[4] a) W. J. Jin , C. Zhang, X. F. Chang, Y. Q. Fan, W. H. Xin, N. P. Xu, *Environ. Sci. Technol.* **2008**, *42*, 3064 – 3068; b) W. Q. Jin, C. Zhang, P. Zhang, Y. Q. Fan, N. P. Xu, *AIChE J.* **2006**, *52*, 2545 – 2550.

[5] a) C. S. Chen, S. J. Feng, S. Ran, D. C. Zhu, W. Liu, H. J. M. Bouwmeester, *Angew. Chem.* **2003**, *115*, 5354 – 5356; *Angew. Chem. Int. Ed.* **2003**, *42*, 5196 – 5198; b) X. Y. Tan, Y. T. Liu, K. L, *AIChE J.* **2005**, *51*, 1991 – 2000; c) Z. P. Shao, W. S. Yang, Y. Cong, H. Dong, J. H. Tong, G. X. Xiong, *J. Membr. Sci.* **2000**, *172*, 177 – 188.

[6] a) H. H. Wang, C. Tablet, A. Feldhoff, J. Caro, *Adv. Mater.* **2005**, *17*, 1785 – 1788; b) X. F. Zhu, H. H. Wang, W. S. Yang, *Chem. Commun.* **2004**, 1130 – 1131; c) K. Watenabe, M. Yuasa, T. Kida, Y. Teraoka, N. Yamazoe, K. Shimanoe, *Adv. Mater.* **2010**, *22*, 2367 – 2370; d) K. Efimov, T. Halfer, A. Kuhn, P. Heitjans, J. Caro, A. Feldhoff, *Chem. Mater.* **2010**, *22*, 1540 – 1544.

[7] a) J. Martynczuk, K. Efimov, L. Robben, A. Feldhoff, *J. Membr. Sci.* **2009**, *344*, 62 – 70; b) M. Arnold, H. H. Wang, A. Feldhoff, *J. Membr. Sci.* **2007**, *293*, 44 – 52.

[8] J. Beckers, G. Rothenberg, *ChemPhysChem* **2005**, *6*, 223 – 225.

[9] C. Zhang, X. Chang, Y. Fan, W. Jin, N Xu, *Ind. Eng. Chem. Res.* **2007**, *46*, 2000 – 2005.

[10] a) I. Kagomiya, T. Iijima, H. Takamura, *J. Membr. Sci.* **2006**, *286*, 180 – 184; b) S. G. Lia, W. Q. Jin, N. P. Xu, J. Shi, *J. Membr. Sci.* **2001**, *186*, 195 – 204; c) J. Sunarso, S. Baumann, J. M. Serra, W. A. Meulenberg, S. Liu, Y. S. Lin, J. C. Diniz da Costa, *J. Membr. Sci.* **2008**, *320*, 13 – 41.

[11] K. Wu, S. Xie, G. S. Jiang, W. Liu, C. S. Chen, *J. Membr. Sci.* **2001**, *188*, 189 – 193.

[12] a) F. T. Akin, Y. S. J. Lin, *J. Membr. Sci.* **2004**, *231*, 133 – 146; b) J. Kim, Y. S. Lin, *J. Membr. Sci.* **2000**, *167*, 123 – 133.

[13] J. E. ten Elshof, N. Q. Nguyen, M. W. den Otter, H. J. M. Bouwmeester, *J. Electrochem. Soc.* **1997**, *144*, 4361 – 4366.

[14] K. Kobayashi, T. Tsunoda, *Solid State Ionics* **2004**, *175*, 405 – 408.

[15] C. S. Chen, Ph.D. Thesis, University of Twente, The Netherlands, **1994**.

[16] a) V. V. Kharton, A. V. Kovalevsky, A. P. Viskup, F. M. Figueiredo, A. A. Yaremchenko, E. N. Naumovich, F. M. B. Marques, *J. Electrochem. Soc.* **2000**, *147*, 2814 – 2821; b) A. L. Shaula, V. V. Kharton, F. M. B. Marques, *J. Electrochem. Soc.* **2004**, *24*, 2631 – 2639; c) V. V. Kharton, A. V. Kovalevsky, A. P. Viskup, A. L. Shaula, F. M. Figueiredo, E. N. Naumovich, F. M. B. Marques, *Solid State Ionics* **2003**, *160*, 247 – 258.

[17] a) Q. M. Li, X. F. Zhu, W. S. Yang, *J. Membr. Sci.* **2008**, *325*, 11 – 15; b) X. F. Zhu, Q. M. Li, Y. Cong, W. S. Yang, *Catal. Commun.* **2008**, *10*, 309 – 312; c) H. H. Wang, W. S. Yang, Y. Cong, X. F. Zhu, Y. S. Lin, *J. Membr. Sci.* **2003**, *224*, 107 – 115.

[18] a) J. X. Yi, Y. B. Zuo, W. Liu, L. Winnubst, C. S. Chen, *J. Membr. Sci.* **2006**, *280*, 849 – 855; b) W. Li, T. F. Tian, F. Y. Shi, Y. S. Wang, C. S. Chen, *Ind. Eng. Chem. Res.* **2009**, *48*, 5789 – 5793; c) B. Wang, M. Zhan, D. C. Zhu, W. Liu, C. S. Chen, *J. Solid State Electrochem.* **2006**, *10*, 625 – 628; d) W. Li, J. J. Liu, C. S. Chen, *J. Membr. Sci.* **2009**, *340*, 266 – 271.

[19] a) K. Efimov, M. Arnold, J. Martynczuk, A. Feldhoff, *J. Am. Ceram. Soc.* **2008**, *92*, 876 – 880; b) A. Feldhoff, M. Arnold, J. Martynczuk, T. M. Gesing, H. Wang, *Solid State Sci.* **2008**, *10*, 689 – 701.

[20] S. Liu, R. Ma, R. Jiang, F. Luo, *J. Cryst. Growth* **1999**, *206*, 88 – 92.

[21] X. F. Zhu, H. H. Wang, W. S. Yang, *J. Membr. Sci.* **2008**, *309*, 120 – 127.

[22] a) J. A. Lane, J. A. Kilner, *Solid State Ionics* **2000**, *136–137*, 927 – 932; b) K. Yashiro, S. Onuma, A. Kaimai, Y. Nigara, T. Kawada, J. Mizusaki, K. Kawwamura, T. Horita, H. Yokokawa, *Solid State Ionics* **2002**, *152–153*, 469 – 476; c) J. E. ten Elshof, H. J. M. Bouwmeester, H. Verweij, *Solid State Ionics* **1996**, *89*, 81 – 92.

[23] J. H. Tong, W. S. Yang, B. C. Zhu, R. Cai, *J. Membr. Sci.* **2002**, *203*, 175 – 189.

[24] V. V. Kharton, E. V. Tsipis, E. N. Naumovich, A. Thursfield, M. V. Patrakeev, V. A. Kolotygin, J. C. Waerenborgh, I. S. Metcalfe, *J. Solid State Chem.* **2008**, *181*, 1425 – 1433.

